



CHORUS

This is the accepted manuscript made available via CHORUS. The article has been published as:

Electron Talbot effect on graphene

Jorge A. Salas, Kalman Varga, Jia-An Yan, and Kirk H. Bevan

Phys. Rev. B **93**, 104305 — Published 29 March 2016

DOI: [10.1103/PhysRevB.93.104305](https://doi.org/10.1103/PhysRevB.93.104305)

The Electron Talbot effect on graphene

Jorge A. Salas and Kalman Varga

Department of Physics and Astronomy, Vanderbilt University, Nashville, TN 37235, USA

Jia-An Yan

Department of Physics, Astronomy, and Geosciences, Towson University, Towson, MD 21252, USA

Kirk H. Bevan

Materials Engineering, McGill University, Montreal, H3A 0C5, Canada

The Talbot effect, employing graphene as a grating and using electron matter-waves, is simulated using Density Functional Theory and solving the Helmholtz equation. Talbot fractional images and long wavelength images are calculated. The results show focusing effects that suggest possible applications for wavepacket reshaping and interferometry.

I. INTRODUCTION

The Talbot effect, also known as self imaging, was discovered in 1836 and many different applications have been developed ever since¹. It is a near field imaging phenomena that takes place by diffracting waves from a periodic grating, with images forming at multiples of the distance Z_T , called the Talbot distance. It has been observed with different types of waves, including matter-waves such as atoms², large molecules³, and electrons^{4,5}. A variety of applications have been developed for acoustics, electron microscopy⁶, x-rays⁷ and photolithography^{8,9}, as well as for interferometry^{3-5,10-14}.

The Talbot images can be obtained by employing grating structures that can be described by discrete spatial frequencies which form concentric rings¹⁵. This is the case for periodic 2D structures. Graphene has recently been the subject of intense research for its optical, mechanical and electronic properties, and it is an ideal candidate for applications utilizing the Talbot effect. Due to its characteristic lengths the imaging of graphene requires short wavelengths, which can be obtained with x-rays or electrons. Graphene-based Talbot effect could find applications in manipulation and control of electron beams, in imaging, and in e-beam lithography or interferometry.

Before Talbot effect in graphene or similar 2D materials can be considered, one has to investigate whether this self interference phenomena is observable for nanometer scale gratings. Experimental studies of electron Talbot effects^{4,5} used 100 nm or larger gratings where electrons scatter from edges rather than from smooth potential energy surfaces of Angstroms resolution. For μm scale gratings, the Talbot effect are nicely described by analytic near field diffraction models¹. We will investigate how well this diffraction model works at the atomistic scale.

In this work we will use Density Functional Theory (DFT) simulations to study the Talbot imaging in graphene by electron diffraction. We will show how the Talbot effect can focus the electron density at different points forming periodic patterns. The calculations also

show Talbot fractional images and long wavelength imaging.

Predicting the Talbot pattern for electrons requires knowledge of the amplitude and phase of the scattered electron wavefunction which depends on the interaction potential between the electron and the graphene. Electron microscopy images are often simulated by employing atomic potentials and form factors, a thorough review can be found in Ref.16. However such models could be limited because bonds between atoms are neglected so a more realistic potential is desirable. In the present work we employ a DFT based approach to simulate Talbot images obtained by scattering electrons from graphene. We have previously used an electron scattering calculation based on DFT for the simulation of electron microscopy images¹⁷, and other groups have also conducted similar simulations¹⁸.

II. CALCULATION

The DFT approach is used to calculate the electron density distribution and realistic electron-target interaction and the Talbot images are obtained by solving the Schrödinger equation for an electron scattering from the self-consistent potential. During the electron scattering, the wave functions of the electrons in the graphene are frozen. In our previous work¹⁷ we have shown that this is a very good approximation for the scattering of electrons. Two energy ranges will be tested. High energies (20 keV) are ideal for Talbot images, because the Fresnel approximation^{14,15} is valid, and as we will show later, one obtains a good resolution of spatial frequencies on the graphene sample with this energy. We will also study the low energy region (80 eV) to see whether or not the Talbot effect can be observed for these less ideal wavelengths.

The calculations are set up in the following way. We place the graphene parallel to the xy plane and use periodic boundary conditions in the x and y directions, with the electron propagating along the z axis. The space is divided into two regions: the first is $z \leq 0$, where

the graphene located, and the second is $z \geq 0$ which is far enough from the graphene so the atomic potential is negligible. This region corresponds to free space where the Talbot effect takes place. The graphene is located at a distance z_0 from the origin (we have tested z_0 in the interval 5 – 7 Å with no effect on the results). For $z \leq 0$ we calculate the wavefunction by time-propagating a wavepacket on a real space grid in the presence of the graphene sheet. The wavepacket has a Gaussian profile along the z direction and it is a plane wave on the xy plane, with periodic boundary conditions,

$$\Psi(x, z, x, t = 0) = \left(\frac{2}{\pi\alpha}\right)^{\frac{1}{4}} e^{ikz - \frac{(z-z_s)^2}{\alpha^2}}, \quad (1)$$

where k is the wave vector, α is the width and $z_s < z_0$ is the center of the initial wave packet. The initial wave packet is time propagated

$$\Psi(x, y, z, t + \Delta t) = \exp\left(-\frac{iH\Delta t}{\hbar}\right)\Phi(x, y, z, t), \quad (2)$$

(the Taylor time propagation is used for the evolution operator), until the wave packet completely passes through the graphene sheet (for low energies (80 eV) there is some reflection from the graphene, for high energy (20 keV) the reflection is negligible, but most of the wave packet transmits through the graphene in both cases). For high energies the wave packet is very oscillatory, and this oscillation can only be approximated on an extremely fine grid (grid spacing less than 0.01 a.u.) , which is computationally unfeasible. In the high energy case we have used the method introduced in our previous work¹⁷ to remove the oscillatory part and allow us to use a grid spacing of $\Delta x = \Delta y = \Delta z = 0.1$ a.u. For the low-energy case one can propagate the wave packet without any problems with a grid spacing of $\Delta x = \Delta y = 0.4, \Delta z = 0.2$ a.u. The wave vector and the width of the wave packets is $k = 2.5, \alpha = 5.7$ and $k = 38, \alpha = 2.7$ a.u. for low energy and high energy, respectively. The actual value of the width is not very important as long as the wave packet can represent the desired energy region.

Once the evolution is complete, the wave function is transformed from the time domain into energy space and the energy resolved wave function with desired energy E ,

$$\Psi_E(x, y, z) = \frac{1}{2\pi} \int \Psi(x, y, z, t) e^{iEt/\hbar} dt, \quad (3)$$

is obtained. In principle, one can use this equation to get the wave function in the entire space, but this would require a long time propagation. Instead, we note that for $z \geq 0$, where the potential is negligible, the Schrödinger equation reduces to the Helmholtz equation and we use this fact to speed up the calculations. After the wave packet has passed beyond the target, we switch from the Schrödinger to the Helmholtz equation. The Helmholtz and the Schrödinger equation are matched by requiring the continuity of the wave function $\Psi_E(x, y, z)$ at $z = 0$, and, in addition, ensuring that the solution remains finite

as z goes to infinity¹⁵. The Helmholtz equation is solved by Fourier transformation on the xy plane¹⁵:

$$\psi_E(x, y, z) = \mathbb{F}^{-1} \left\{ \mathbb{F} \{ \psi_E(x, y, 0) \} e^{i\kappa z} \right\}, \quad (4)$$

with $\kappa = 2\pi\sqrt{\frac{1}{\lambda^2} - \xi^2}$, where λ is the de Broglie wavelength and ξ the spatial frequency on the xy plane. Solving the problem this way, that is by splitting space into two regions, is computationally less expensive than time propagating the wavepacket numerically in the entire space.

By Fourier transforming $\psi_E(x, y, 0)$ to frequency space, one can visualize the Montgomery rings¹⁴. Figure 2 shows that the allowed spatial frequencies of $\mathbb{F} \{ \psi_E(x, y, 0) \}$ form concentric rings, which is a necessary condition for self-imaging¹⁵, while the others have negligible amplitudes. The radii of the rings in Fig.2 are in good agreement with the values deduced from the reciprocal lattice vectors of graphene¹⁹.

We have investigated the self-imaging in two limiting cases, for high energy $E = 20$ keV and for low-energy $E = 80$ eV. One advantage of using high energy is that the Talbot distance (inversely proportional to the wavelength) is larger which could make it easier to measure experimentally. On the other hand imaging with low energy can have some bandwidth limitations¹⁵ and while the Talbot distance is shorter it might be more sensitive to the electron distribution in graphene.

Figure 3 shows the one dimensional electron density profile on the z direction for $E = 20$ keV along lines that pass through a carbon atom, carbon bond and the center of a hexagon (see also in Fig.1). The figure shows that the electron density is periodically repeated with a Talbot distance of $Z_T = 104$ Å, but the intensity distribution depends on the x, y coordinates. The calculated Talbot distance is in good agreement with the prediction for hexagonal lattices¹⁹ ($Z_T = 3a^2/2\lambda$, with $a = 2.46$ Å). The Talbot carpet, the density distribution on the xz plane (see Fig.4), shows similar periodic density enhancements.

The Talbot image, the electron density on the xy plane, at $Z = 0$ (and $z = Z_T$), is shown in Fig. 5a. The density is higher at points that match the positions of the carbon atoms, so the image resembles that of the graphene sheet. The rings around the image of atomic positions are broken into higher and lower intensity regions.

Next we show the fractional Talbot images at $1/2Z_T$, $1/3Z_T$, $2/3Z_T$, and $1/6Z_T$. At $z = Z_T/2$, shown in Fig. 5b, the pattern resembles the original graphene (darker spots) but has smaller concentric honeycombs inside (lighter spots) with a higher intensity than the original ones, at a distance of $1/2$ the radius of the honeycomb.

Different focusing effects can be obtained at $z = Z_T/3$, shown in Fig. 5c, where there is a high intensity pattern around the original graphene honeycomb positions and low intensity in the centers. For $z = 2/3Z_T$, (Fig. 5d) , the situation is reversed since now the honeycomb centers

have high intensity and the carbon atoms' positions are darker. The density has its intensity maximum (about 1.55, see Fig. 3) and highest localization (highest amplitudes concentrated in smaller regions) on this plane ($z = 2/3Z_T$). This localization may have applications in electron pulse reshaping and interferometry. Finally, at $z = 1/6Z_T$ (Fig. 5e), spatial density oscillations are obtained along the carbon bonds, with a period of half a bond length. The hexagon centers correspond to the darker regions in the figure, while the brighter areas correspond instead to the midpoints of the carbon bonds.

In the low energy case, we have used $E = 80$ eV, which has a wavelength $\lambda = 1.37$ Å. This allows a resolution of spatial frequencies up to about $\xi = 0.74$ Å⁻¹. This is only sufficient to resolve the first Montgomery ring, shown in Fig.2 $\xi \approx 0.47$ Å⁻¹, so only coarse details of the graphene structure are included. The grid spacing is about 0.4 in xy and 0.2 a.u. in z . Since the Fresnel approximation is no longer valid the Talbot distance must be obtained

from $Z_T = \frac{\lambda}{1 - \sqrt{1 - \lambda^2 \xi^2}}$ (derived from Ref.15) which

for the first ring of radius ξ gives $Z_T = 5.8$ Å, in good agreement with the calculated results shown in Fig. 6. Note that in this case the simulation cell is small and thus there is no need to use the Helmholtz equation to reduce computational costs. Therefore the density can be obtained directly from the solution of the Schrödinger equation. Fig. 6 shows that the relative intensity for passing through the center of the honeycomb is much higher than that passing through the atoms' positions. The relative amplitude in this case goes up to about 6, in contrast with our $E = 20$ keV case where it was only around 1.6 at the most. Also, in this case the peaks for the honeycomb center and the atoms are completely out of phase. At the position of these peaks we obtained focusing of the electron density towards the center of the hexagons, shown in Fig.5f, which is a similar pattern to the one obtained for $E = 20$ keV at $z = 2Z_T/3$.

III. SUMMARY AND DISCUSSION

In summary, we have shown that graphene can be used to focus electron wavepackets exploiting the Talbot self-imaging effect, creating periodic images with various patterns. While the Talbot effect has been well-known and applied for many different waves, here we have shown that electron Talbot self interference can be generated even with Angstrom scale gratings of 2D materials. The atomistic effects, presence of extended charge distributions and potentials, or screening do not hamper the self interference. The Fresnel approximation with point like scatterers¹⁹ gives a good approximation for the Talbot distances, for a more quantitative picture, however, one needs a simulation that incorporates the atomistic features as well.

By choosing the proper wavelength, one can adjust the Talbot distances and intensities, maximizing electron lo-

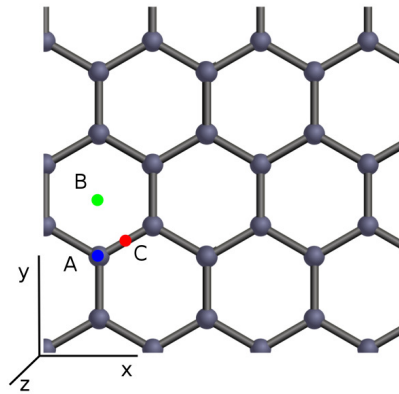


FIG. 1. Graphene reference points used: (A) Carbon atom , (B) Hexagon center (C) Bond. The electron propagates along the z axis.

calization at certain points which could be useful for wavepacket manipulation or e-beam lithography. Further investigation is needed to study the effects of beam characteristics in space and time, sample size, and perturbations to the graphene (e.g. the presence of defects or wrinkles).

The question is how can be this effect observed experimentally. The Talbot distance for 20 keV electrons is small, about 10 nm. One can increase the Talbot distance (proportional to $1/\lambda$) by increasing the energy, but higher energies may damage the graphene.

Another possibility is to use an interferometer as it has been suggested in⁴, where the Talbot effect is observed with the help of a second grating (e.g. bilayer graphene). One can also speculate about a possible use of graphene for angular Talbot effect²⁰, where point source illumination is used to produce far field angle dependent Talbot interference images.

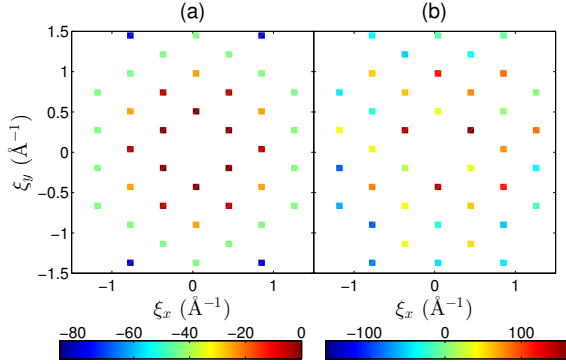


FIG. 2. Montgomery rings for graphene, obtained using a FFT on ψ_E at $z = 0$, with spatial frequency components ξ_x and ξ_y in \AA^{-1} . (a) Amplitude (in dB) of the spatial frequencies, normalized to the average amplitude of the first ring, and (b) phase (degrees) of each spatial frequency component. The zeroth ring has been removed from the graph, but not from the calculations.

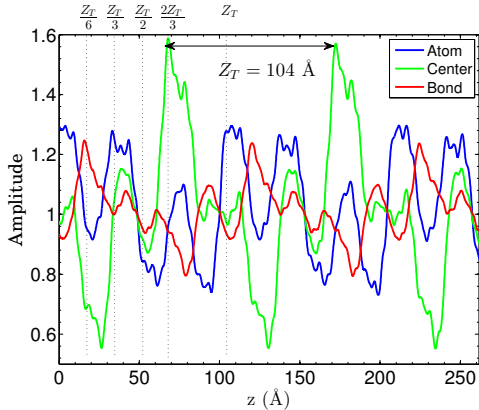


FIG. 3. Electron density profiles in the z direction, corresponding to 20keV, passing through the reference points specified in Fig.1. The amplitudes shown are normalized respect to the free space transmitted density, obtained if the graphene grating was absent in the simulation. The obtained Talbot distance is about 104\AA . The vertical lines correspond to the planes where the density was studied, at fractional Talbot distances, shown in subsequent figures.

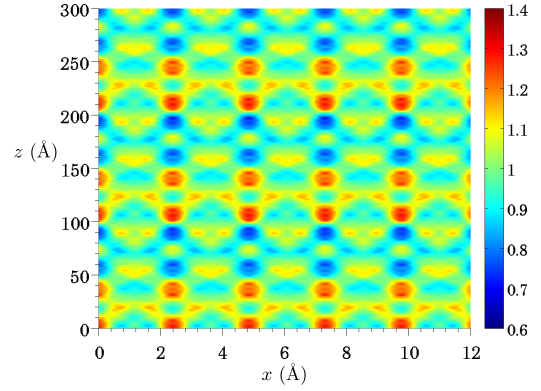


FIG. 4. The density along a plane parallel to the xz plane is shown. In this case the plane passes through a carbon atom at $x,z=0$. Amplitudes are normalized respect to free space transmission.

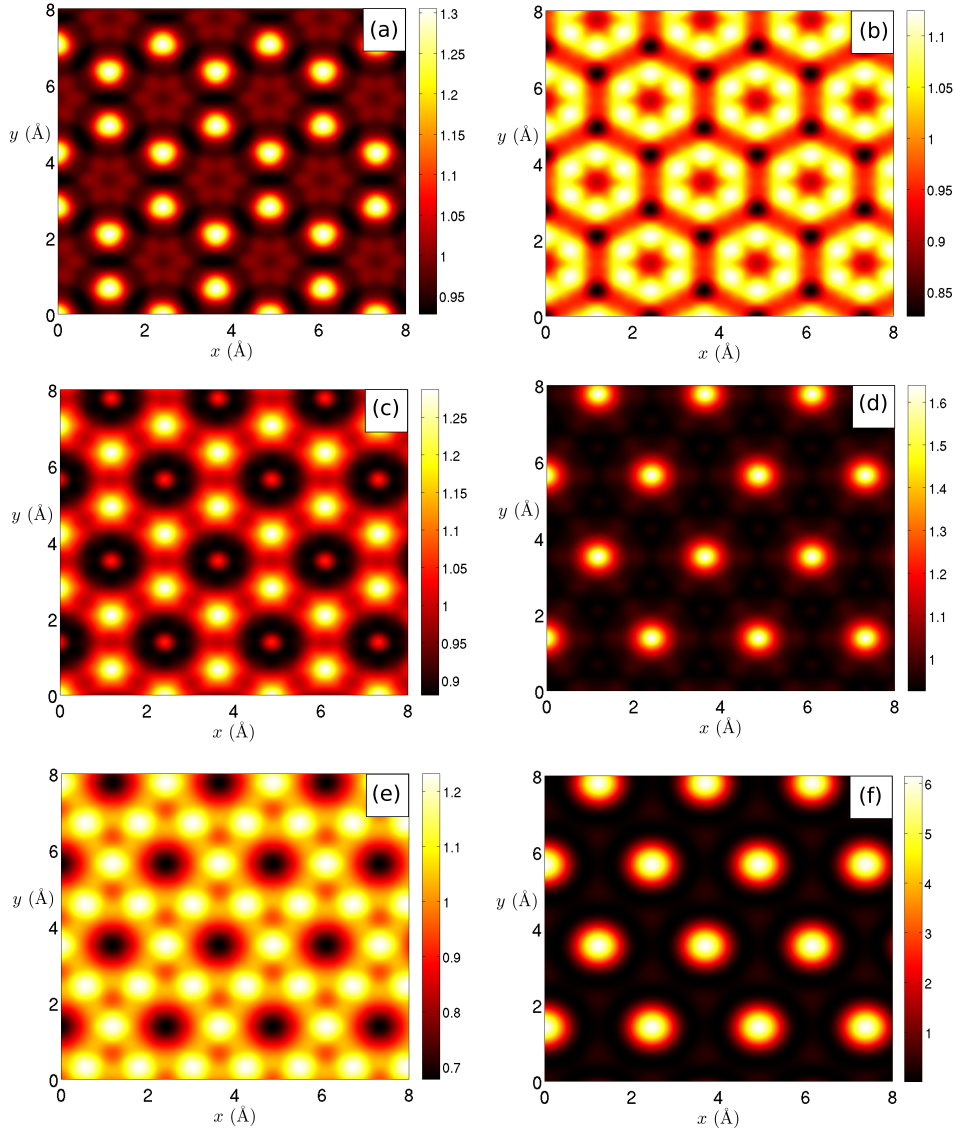


FIG. 5. Density on the xy plane for different values of z , as shown in Fig.3. Amplitudes are normalized respect to free space transmission. The 20keV cases are depicted from (a) to (e), while (f) corresponds to 80eV.

(a) $z = 0$ or $z = Z_T$. The points with highest intensity overlap with the centers of the carbon atoms, so this image resembles the graphene to its original scale. The origin coincides with point A marked in Fig.1.

(b) $z = \frac{1}{2}Z_T$. Here we obtain smaller hexagons with length $1/2$ the original ones. The darker spots correspond to the original locations of the atoms. These points are now vertices of smaller hexagons, delimited by the newly arised bright spots located inside the honeycombs in the midpoint between the bond and the center.

(c) $z = \frac{1}{3}Z_T$.

(d) $z = \frac{2}{3}Z_T$. The points with highest intensity overlap with the centers of the graphene honeycombs.

(e) $z = \frac{1}{6}Z_T$.

(f) Density for the 80eV case, at the points in z where the density reaches its maximum value at the centers of the honeycombs, as shown in Fig.6.

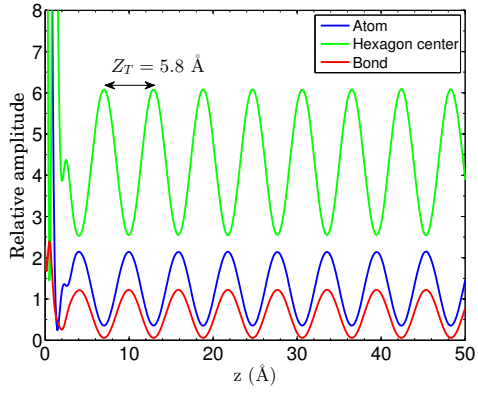


FIG. 6. Electron density profiles, corresponding to an energy of 80eV, along parallel lines to the z axis, passing through the reference points specified in Fig.1. The obtained Talbot distance is about 5.8Å. In this case the graphene sheet is placed at $z=0$.

ACKNOWLEDGMENTS

This work has been financed by the National Science Foundation (NSF) under grants No.Phy 1314463 and No.IIA126117. The authors would like to thank Daniel Kidd and Arthur Russakoff for their suggestions for the writing of this manuscript.

-
- ¹ J. Wen, Y. Zhang, and M. Xiao, *Adv. Opt. Photon.* **5**, 83 (2013).
 - ² M. S. Chapman, C. R. Ekstrom, T. D. Hammond, J. Schmiedmayer, B. E. Tannian, S. Wehinger, and D. E. Pritchard, *Phys. Rev. A* **51**, R14 (1995).
 - ³ B. Brezger, L. Hackermüller, S. Uttenthaler, J. Petschinka, M. Arndt, and A. Zeilinger, *Phys. Rev. Lett.* **88**, 100404 (2002).
 - ⁴ B. J. McMorran and A. D. Cronin, *New Journal of Physics* **11**, 033021 (2009).
 - ⁵ R. Bach, G. Gronniger, and H. Batelaan, *Applied Physics Letters* **103**, 254102 (2013).
 - ⁶ J. M. Cowley and A. F. Moodie, *Proceedings of the Physical Society. Section B* **70**, 486 (1957).
 - ⁷ T. Weitkamp, A. Diaz, C. David, F. Pfeiffer, M. Stambanoni, P. Cloetens, and E. Ziegler, *Opt. Express* **13**, 6296 (2005).
 - ⁸ H. H. Solak, C. Dais, F. Clube, and L. Wang, *Microelectronic Engineering* **143**, 74 (2015).
 - ⁹ T. Sato, A. Yamada, T. Suto, R. Inanami, K. Matsuki, and S. Ito, *Microelectronic Engineering* **143**, 21 (2015).
 - ¹⁰ A. Lohmann and D. Silva, *Optics Communications* **2**, 413 (1971).
 - ¹¹ A. Lohmann and D. Silva, *Optics Communications* **4**, 326 (1972).
 - ¹² M. P. Valdivia, D. Stutman, and M. Finkenthal, *Review of Scientific Instruments* **85**, 073702 (2014).
 - ¹³ A. D. Cronin, J. Schmiedmayer, and D. E. Pritchard, *Rev. Mod. Phys.* **81**, 1051 (2009).
 - ¹⁴ K. Patorski, in , *Progress in Optics*, Vol. 27, edited by E. Wolf (Elsevier, 1989) pp. 1–108.
 - ¹⁵ W. D. Montgomery, *J. Opt. Soc. Am.* **57**, 772 (1967).
 - ¹⁶ E. Kirkland, in *Advanced Computing in Electron Microscopy* (Springer US, 2010) pp. 243–260.
 - ¹⁷ J.-A. Yan, J. A. Driscoll, B. K. Wyatt, K. Varga, and S. T. Pantelides, *Phys. Rev. B* **84**, 224117 (2011).
 - ¹⁸ K. Tsubonoya, C. Hu, and K. Watanabe, *Phys. Rev. B* **90**, 035416 (2014).
 - ¹⁹ L.-W. Zhu, X. Yin, Z. Hong, and C.-S. Guo, *J. Opt. Soc. Am. A* **25**, 203 (2008).
 - ²⁰ J. Azaña and H. Guillet de Chatellus, *Phys. Rev. Lett.* **112**, 213902 (2014).